# Influence of Copper Doping on Structural, Morphological, Electrical Properties of WO$_3$ Nanoparticles

R. Priya[1*], R. Balan[2]

[1]Department of Physics, Info Institute of Engineering, Coimbatore, TN, India
[2]Department of Physics, Chikkanna Government Arts College, Tirupur, TN, India
Received: 22.02.2018        Accepted: 27.03.2018        Published: 30-06-2018
*priyakce08@gmail.com

## ABSTRACT

In this work, Pure and Cu-doped WO$_3$ nanoparticles have been synthesized using the wet chemical method. The effect of Cu-doping on the structural, morphological, electrical and dielectric properties of WO$_3$ nanoparticles was investigated. XRD pattern described that Cu-doping without affecting the monoclinic structure of the samples and the few peaks corresponding to Cu, it conforms secondary phase. The presence of more distortion centers and interstitials in Cu-doped sample led to increasing the crystallite size. FESEM analysis has shown the morphology of doped and pure WO$_3$ nanoparticles to be quasi-spherical. EDAX spectra confirmed the presence of W, O and Cu. The DC and AC conductivity have been measured at a temperature range from 303-403K in the frequency range of 42Hz-5MHz. The DC conductivity was found to increase with increasing Cu and indicates the semiconducting nature. The activation energy has also been observed to decrease with Cu doping. The DC conductivity of the present samples follows small polaron hopping. The frequency dependence of dielectric constant ($\varepsilon'$), dielectric loss (tan $\delta$) and AC conductivity of WO$_3$ nanoparticles of different Cu doping concentration at different temperature was measured. Temperature variation of frequency exponents in 15 wt% Cu-doped WO$_3$ suggests that AC conduction is attributed to be correlated barrier hopping.

**Keywords:** Cu-doped WO$_3$; Dielectric study; Electrical conductivity; FESEM; XRD.

## 1. INTRODUCTION

Tungsten oxide (WO$_3$) is one of the most important transitions metal oxide n-type semiconductors with a bandgap of 2.7 eV. It has many excellent properties, such as non-toxic, cheap, unique optical and electrical properties, which has a wide range of applications in the field of the sensor, smart windows, electrochromic, photocatalysts and photodetector (Wen Zeng *et al.* 2014; Georg *et al.* 2008; Danine*et al.* 2014; Changhua *et al.*2014; Zhiyang He *et al.*2015). A number of methods have been employed for doped transition metal oxide nanoparticles with different sizes and shapes, such as colloidal chemical, template, RF thermal plasma, sol−gel, screen printing, chemical co-precipitation (Huijuan Xia *et al.* 2008; Hui Song *et al.*2015; Mingshui Yao *et al.* 2015; SomayehFardindoost*et al.* 2010; Hubalek*et al.* 2004; Upadhyay*et al.* 2014) and so on. Among these methods, the wet chemical method seems to be a versatile, low-cost, and environmentally friendly method for preparing WO$_3$ nanostructures. To date, properties of WO$_3$ can be tuned according to the research interest by doping with various metal atoms to proper pre-determined needs and applications (Wang *et al.* 2007). The metal dopant induces a significant modification in the optical and electrical properties of WO$_3$. Numerous researchers have reported the changes induced by the incorporation of transition metal ions into WO$_3$ lattice (Huijuan Xia *et al.* 2008; Kuzmin*et al.* 2014; Ahsan *et al.* 2012; Cholsong Pang *et al.* 2010; Gaury*et al.* 2013).

In the few decades, the number of reports on transition metal doped WO$_3$ system, very fewer work is done on Cu-doped WO$_3$. The main reason for choosing dopant Cu to act as an electron receptor offers electrons to the WO$_3$ conduction band and changes the electronic structure and carrier concentration of the metal oxide. Particularly, Cu is an equivalent substance in WO$_3$ and so far enhances electrical conductivity (Wang, 2011). For example, the doping of Cu occupies the atomic sites instead of interstitial sites of the WO$_3$ lattice. Therefore, Cu incorporation WO$_3$ photonic crystal structure exhibit enhanced sensitivity to TMA (to check the freshness of fish) compared with the pure WO$_3$(Shenmin Zhu *et al.* 2010). The Cu-doped WO$_3$ found that the sensing properties of acetone gas have been significantlyimproved compared with undoped WO$_3$(Hao Zhou *et al.* 2015).

Many researchers have been interested investigate the dielectric properties of WO$_3$ and AC measurements, which is an important tool for studying

properties like dielectric constant, dielectric loss tangent, capacitance and semiconducting dielectric materials (El-Nahass *et al.* 2012; Hutchins *et al.* 2007). This measurement gives information about the interior of the material. Besides, a given material dielectric properties strongly depend on the preparation conditions. Therefore, the present investigation deals with the structural, morphology, electrical and dielectric properties of Cu-doped $WO_3$ nanoparticles with Cu content are varying from 5 to 15 wt% via the wet chemical method. The electrical properties of Cu influence $WO_3$ have also been investigated.

## 2. MATERIALS & METHODS

### 2.1 Chemicals

In this experiment, all chemicals were used analytically grade and without further purification. All the solutions were prepared in deionized water. Sodium tungstated dehydrate ($Na_2WO_4.2H_2O$), hydrochloric acid (HCl), Copper (II) chloride dihydrate ($CuCl_2 \cdot 2H_2O$), PVP ($C_6H_9NO)_n$, CTAB(($C_{16}H_{33})N(CH_3)_3Br$), oxalic acid ($C_2H_2O_4.2H_2O$) were used as precursors, dopant source, and solvent respectively.

### 2.2 Synthesis of $WO_3$ and $Cu_xWO_3$ Nanoparticles

The modified structures of tungsten trioxide nanoparticles doped with Cu were prepared by a wet chemical method. Initially, an appropriate amount of sodium tungstate dihydrate was dissolved in 20 ml of deionized water and stirred for 10-20 min. The solution was acidified to a pH value of 1.0 by slowly adding HCl under continuous stirring. A white precipitated solution was obtained, and it was added by oxalic acid. Then, the white precipitation solution was immediately changed to the transparent solution. After that, the transparent solution was changed to pale white color while adding CTAB. Upon introduction of PVP, the pale white color solution was changed into yellow color. Finally, 5, 10 and 15 wt% of copper (II) chloride dihydrate was dissolved in 10 ml of deionized water and then added to the resultant solution under magnetic stirring heated to 80°C for 1h, to ensure complete reaction. After the process was completed, resulting bluish-green precipitation were vigorously stirring for 24h at room temperature. To remove by-product, the obtained resultant precipitation was washed much time with ethanol, acetone and deionized water, filter and then dried in an oven at 180°C for 6h and to collect the as-prepared sample. Then dried products were annealed at 400°C in the muffle furnace. The color of bluish green as the prepared sample changed into the dark green sample during annealing. Hereafter, annealed copper doped tungsten oxide can be referred to as $Cu_xWO_3$ (x= 5, 10 and 15 wt%). A similar method of preparation without the addition of Cu was used to synthesize a pure $WO_3$ sample.

### 2.3 Material Characterization

The crystallographic information of Cu-doped $WO_3$ was obtained through X-ray diffraction (Bruker AXS D8 advance X-ray diffraction) and Field Emission Scanning Electron Microscope (FEI Quanta FEG-200) attached with energy dispersive spectrometer (EDX) at room temperature. DC electrical conductivity of pellet form of samples coated with silver paste on both surface was studied via a Keithley6517B. In addition, dielectric parameters and AC conductivity were obtained as a function of frequency (42Hz - 5MHz) at different temperatures using a computer-controlled-LCRHI Tester (HIOKI3532-50).

## 3. RESULTS AND DISCUSSION

### 3.1 Morphology and Structural Characterization

Fig. 1(a) shows XRD patterns of wet chemically synthesized 5, 10 and 15 wt% Cu-doped $WO_3$ together with pure $WO_3$. As shown in Fig 1a, several significant diffraction peaks (23.32°, 24.14°, 27.20°, 28.13°, 29.36°, 34.98°, 42.85° and 46.90°) could correspond to were observed for $WO_3$, characteristic of monoclinic $WO_3$ (JCPDS no. 72-1465). All $Cu^{2+}$ doped $WO_3$ exhibit some additional peaks at the angle 18.83° and 31.77° about 2θ corresponding to $Cu_2WO_4$ (indexed by *) phase, which was confirmed from JCPDS card no.78-0928. It was observed that, as the concentration of $Cu^{2+}$ doping increases, additional peak's intensity also increases. The presence of secondary $Cu^{2+}$ phase in our samples confirms the limit of substitutional incorporation of $Cu^{2+}$ ions into $WO_3$. The broadening of the peaks is responsible for the formation of particles in the nanometer regime (Hui Song *et al.* 2015). From Fig.1(b), it was noticed that the diffraction peaks shift slightly towards higher angles for all $Cu^{2+}$ doping concentrations, which is due to the occupancy of $W^{6+}$ (0.78 Å) sites by $Cu^{2+}$(0.73Å), causing some kind of lattice distortion that is induced by the stress during the preparation (Jonscher, 1983). The crystallite size (D), calculated using Scherrer's formula:

$$D = \frac{0.89\lambda}{\beta \cos\theta} \quad (1)$$

where λ is the wavelength of incident X-ray, β is the full width at half maximum (FWHM) of the diffraction peak, and 2θ is diffraction angle. It can be noticed that the value of crystallite size increases with increasing $Cu^{2+}$ doping are listed in Table 1. This may be due to lattice strain induced in the doped $WO_3$ caused by the small mismatch of ionic radii between the host $W^{6+}$ and dopant $Cu^{2+}$.
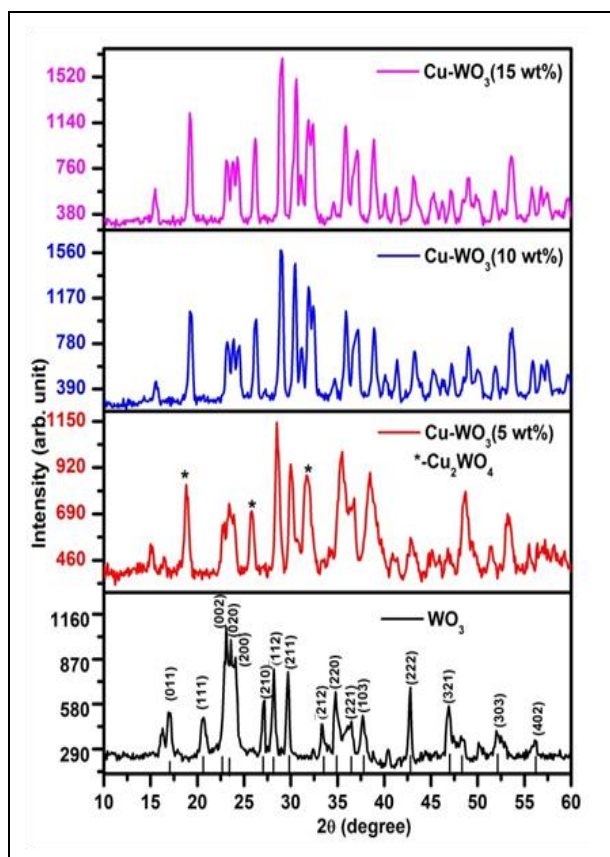
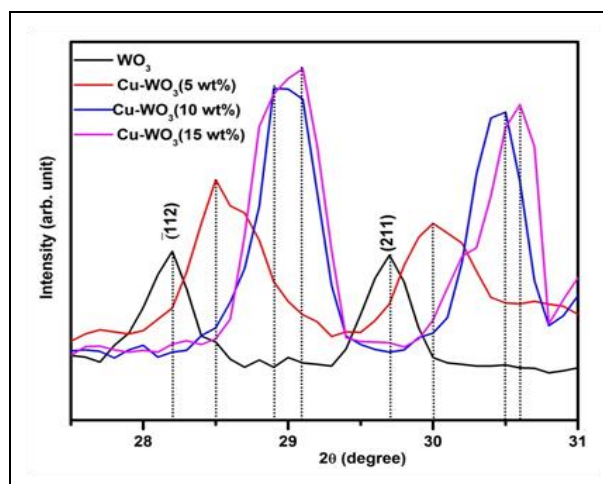Fig. 1a: XRD of WO₃ and Cu doped WO₃ calcined at 400 °C.



**Fig. 1b: Comparison of the (221) and (112) peaks taken for WO₃ and Cu doped WO₃**

The shifting of XRD peaks and corresponding to increase of crystallite size suggest that $Cu^{2+}$ ions are successfully incorporated into the WO₃ without altering the overall crystal structure.

### 3.2 Microstructure and Compositional Studies

The FESEM measurements were carried out to confirm the nature of nanoparticles and to study the morphology of the particles. Fig. 2a–d shows the morphology of pure and $Cu_xWO_3$ nanoparticles (x = 5, 10 and 15 wt%) annealed at 400 °C, respectively. The occurrence of particles is inhomogeneous and more compact structure. Also, the surface of the layer is covered with irregular distribution of particles structure.

**Table 1. Summary of crystallite size and electrical conductivity of pure and copper doped WO₃**

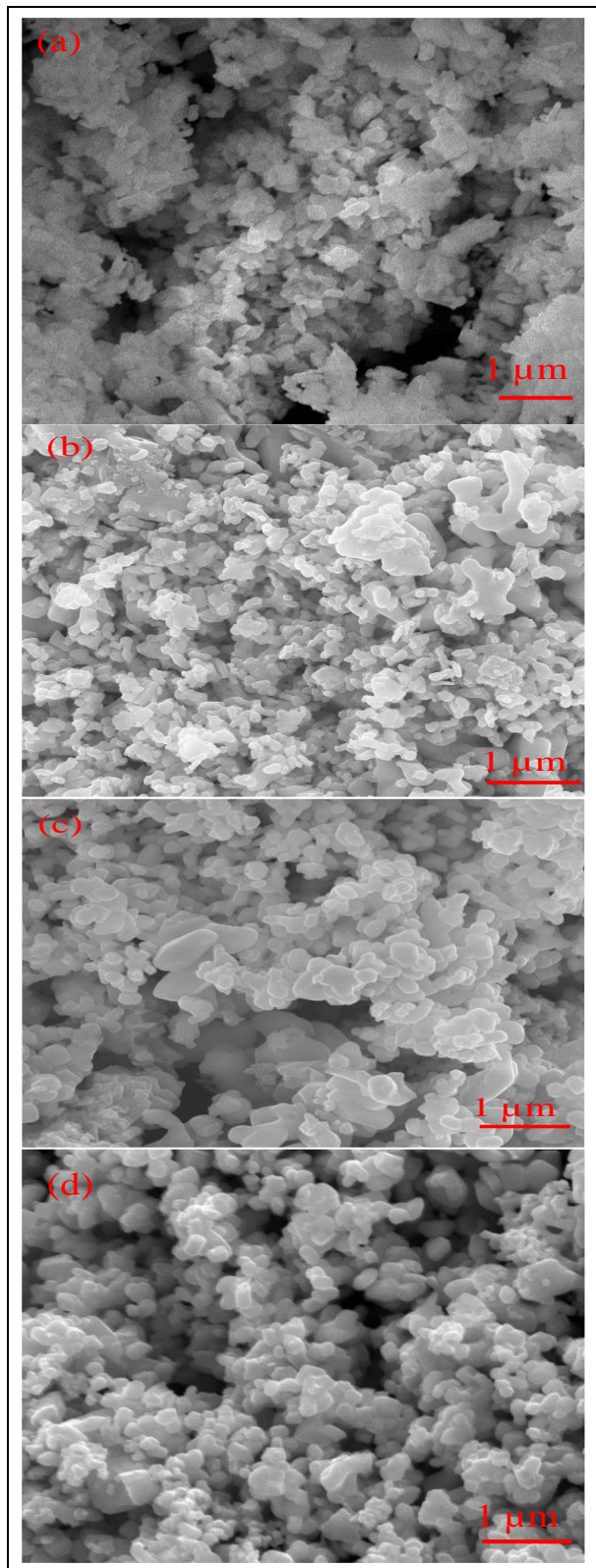| Samples | Crystallite size (β) (nm) | DC characterization | | AC characterization | | | |
|---|---|---|---|---|---|---|---|
| | | $\sigma_{dc}$ (S/cm) | $E_a$ (eV) 383-393 K | $\sigma_{ac}$ (S/cm) at 1 MHz | $E_a$(eV) 383-393 K | Dielectric constant ($\varepsilon'$) | Dielectric loss (tan δ) |
| Pure WO₃ | 15.57 | $9.04 \times 10^{-8}$ | 0.98 | $5.06 \times 10^{-5}$ | 0.55 | 2717 | 6.12 |
| Cu- WO₃ (5 wt%) | 16.67 | $3.49 \times 10^{-7}$ | 0.35 | $5.94 \times 10^{-5}$ | 0.34 | 359 | 4.18 |
| Cu- WO₃ (10 wt%) | 17.27 | $2.47 \times 10^{-6}$ | 0.34 | $2.54 \times 10^{-5}$ | 0.24 | 391 | 2.21 |
| Cu- WO₃ (15 wt%) | 18.81 | $1.29 \times 10^{-5}$ | 0.33 | $2.85 \times 10^{-5}$ | 0.42 | 480 | 2.83 |

**Fig. 2: FESEM image of (a) WO3 (b) 5 wt% Cu doped WO3(c) 10 wt% Cu doped WO3 and (d) 15 wt% Cu doped WO3.**

Fig. 2a shows the surface morphology of pure $WO_3$ nanoparticles, which has agglomerated irregular particle structure. The morphology of the $Cu_5WO_3$

sample is shown in Fig. 2b. It was observed that the irregular particles' structures disturbed by Cu-doping not altering the morphology of pure $WO_3$ nanoparticles. The further addition of 10 and 15 wt% of Cu into $WO_3$ improves the crystal structure quality of the samples, as shown in Fig. 2c-d. FESEM is revealed the formation of quasi-spherical nanoparticles with non-uniform particle size distribution. The presence of $WO_3$ phase and interstitials/vacancies made by Cu = 15 wt% sample particle size is higher than the sample with Cu = 5 wt% and 10 wt%. The quality of $WO_3$ sample is increased by increasing wt% of Cu. However, the appeared particle structure depends on the dopant concentration.

The presence of elements and purity of the samples is confirmed through EDX spectra. Fig. 3 the spectra indicate the atomic percentage of the compositional elements such as W, Cu, O and C, respectively. It proves the presence of Cu in $WO_3$ lattice.
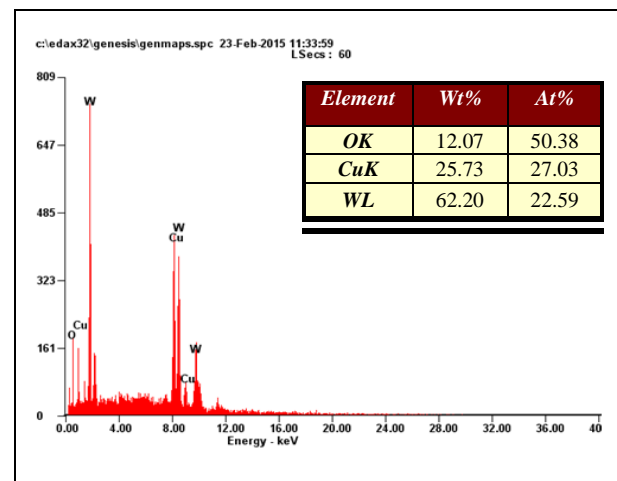


| Element | Wt% | At% |
|---------|-------|-------|
| OK | 12.07 | 50.38 |
| CuK | 25.73 | 27.03 |
| WL | 62.20 | 22.59 |

**Fig. 3: EDAX spectra of 15 wt% Cu doped WO₃**

## 3.3 Electrical Conductivity

The understanding of the conductivity represents the dynamic behaviour of ion in the conducting materials. The conductivity value at low-frequency spectra are frequency independent and are shown as DC conductivity. The temperature dependence of the dc conductivity gives information about the long time ion dynamics, and it is described by well known Arrhenius law, reflecting the activated nature of electron hopping processes. At high frequencies, the conductivity becomes strongly frequency-dependent. The total measured conductivity ($\sigma_T$), is related to the DC conductivity $\sigma_{dc}$, and the component $\sigma_{ac}$ of the materials was first reported by Jonscher power law (Jonscher, 1983) as

$$\sigma_T = \sigma_{ac} + \sigma_{dc} = A\omega^s \qquad (2)$$

where $\sigma_{dc}$ is DC conductivity is frequency independent, A is a constant, s is the exponent of frequency (s<1), and $\omega$ is the angular frequency of the applied field ($\omega=2\pi f$). The above equation explains the measured AC conductivity $\sigma_T$ increases by 3–4 orders of magnitude of DC conductivity ($\sigma_{dc}$). Hence, the measured value of total conductivity $\sigma_T$ has depended on the typical values of AC conductivity. The real part of AC conductivity obeys the following relation:

$$\sigma_{ac} = \varepsilon_0 \omega \varepsilon' \tan \delta \qquad (3)$$

where $\varepsilon' = \dfrac{Cd}{\varepsilon_0 A}$ $\tan \delta = \dfrac{\varepsilon''}{\varepsilon'}$ and, defines dielectric constant and loss tangent, $\varepsilon_0$ is the free space permittivity, and A is an area of the pellet, and d is the thickness of pellet samples. The value of $\tau\eta\varepsilon$ $\sigma_{ac}$ is depended on the frequency, temperature and composition of the sample.

### 3.3.1 DC electrical conductivity ($\sigma_{dc}$)

WO$_3$ is a well-known n-type semiconductor. The electrical conductivity is linked with tungsten interstitials and oxygen vacancy (intrinsic defects) present in WO$_3$. These defects introduce donor states in the forbidden band slightly below the conduction band, thus resulting in the conducting behavior of WO$_3$. The electrical conductivity of the sample is controlled by the intrinsic defects generated during synthesis and by the presence of dopant. Simpson and Cordero (Simpson and Cordaro, 1988) have reported electrical conductivity of the sample at room temperature is caused by oxygen vacancy. Thus, the electrical conductivity ($\sigma_{dc}$) of the pure and wt% of copper doped WO$_3$ for different temperatures in the range 303–403 K with an increment of 10 K has been calculated by the formula:

$$\sigma = \frac{1}{\rho} = \frac{VA}{Id} \qquad (4)$$

where V is the applied voltage, I is the measured current, A is the pellet area, and d is the pellet thickness. Fig.4a reveals that the electrical conductivity has been found to increase with the increase of temperature for both pure and doped WO$_3$, and the values lie in the order of $10^{-8}$–$10^{-5}$ S cm$^{-1}$ i.e., indicating a semiconducting nature of all the samples. At higher temperature region, the carrier concentration increases due to intrinsic thermal excitation and electron emission. At lower temperatures, the probability of thermal excitation becomes quickly smaller so that the charge carrier hops to a neighbouring localized state (Gartstein and Conwell, 1995). The electrical conductivity of WO$_3$ is increased with an increase in Cu concentration. This can be explained on the basis of a smaller conductivity of copper ($5.8\times10^5\Omega$cm) than that of ($1.79 \times10^5\Omega$cm).

The temperature dependence of conductivity can be represented by the well-known Arrhenius equation, given by

$$\sigma_{dc} = \sigma_o \exp\left[\frac{-E_a}{RT}\right] \qquad (5)$$

where $\sigma_0$ is the pre-exponential factor, $E_a$ is the thermal activation energy, R is the ideal gas constant, and T is the temperature in Kelvin.
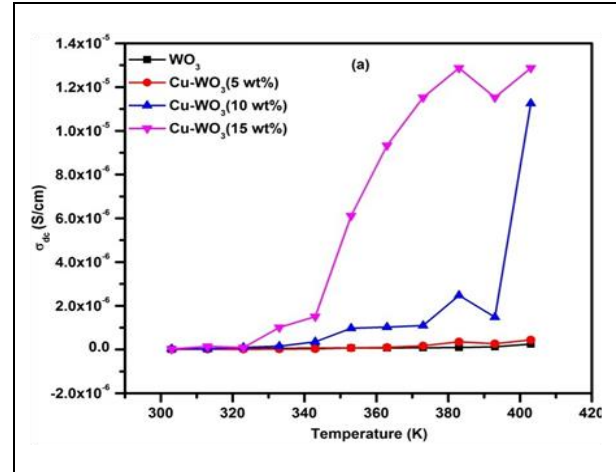


**Fig. 4a: Temperature-dependent DC electrical conductivity of WO$_3$ and Cu doped WO$_3$**

Fig. 4b shows the plots of the $\ln\sigma_{dc}$ versus $10^3/T$ (K$^{-1}$) for pure and doped WO$_3$. The activation energy has been calculated using the slope of this figure for each sample. Activation energy has been found to decrease with an increase of copper content presented in Table 1. When WO$_3$ is doped with Cu, then Cu atoms replace W atoms which can be easily ionized because of the smaller ionization potential of Cu than that of W. Therefore, the DC electrical conductivity of WO$_3$ is increased by increasing Cu doping and the corresponding decrease in activation energy is found to be associated with a shift of Fermi level in doped samples (Shumaila*et al.* 2011). Another attempt has also been made to confirm the nature of hopping conduction and observe the strength of the interaction of electron-phonon. We have fitted temperature dependence resistivity data with the small polaron hopping model given by Mott and Davis (Mott and Davis, 1979). It is also found that high-temperature transport properties in the rare-earth transition metal oxide systems are dominated by the thermally activated hopping of small polaron. The increase in temperature causes the electrons to acquire enough energy and cross or trapped adjacent atoms or ions site. Thus, in the high-temperature region, the electrical conductivity of pure and Cu-doped WO$_3$ is thermally activated from the donor level to the conduction band due to the small polaron hopping process.
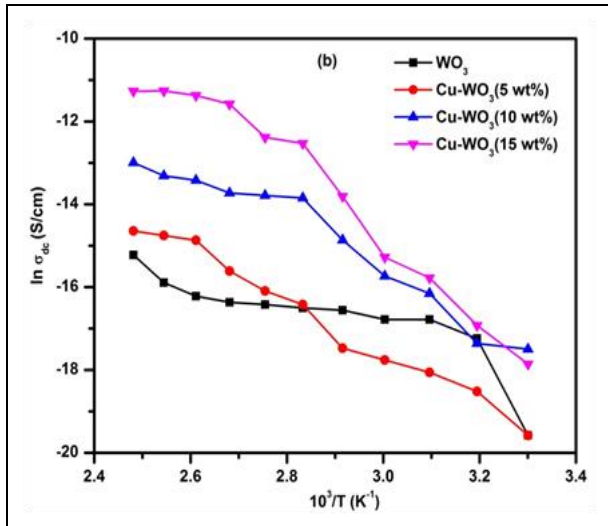
**Fig. 4b: Arrhenius plot lnσdc versus T1/3 for WO₃ and Cu doped WO₃**

### 3.3.2 AC conductivity (σ ac)

The measurement of frequency dependence of AC conductivity is providing information about the nature of charge carriers. The relation between the AC conductivity and the frequency at different temperature for the pure and doped $WO_3$ under investigation is plotted as lnf versus $\sigma_{ac}$. The frequency-dependent of AC conductivity value is weak at lower frequencies, and thenit increases rapidly at higher frequencies. Therefore, the electrical conduction in the sample takes place via a hopping mechanism. It is also clear from Fig. 5a-5d that the maximum conductivity is obtained for pure $WO_3$, which decreases with increasing wt% of Cu doping in $WO_3$. This decrease in AC conductivity can be explained by the fact that Cu ions produce defects such as oxygen vacancies and tungsten interstitials in the $WO_3$ host system. These defects tend to segregate at the grain boundaries. Therefore, the defections increased by increasing Cu doping which facilitates the formation of defect barrier in the grain boundary leading to the blockage of the flow of charge carriers. This, in turn, decreases the conductivity of $WO_3$ on doping. The values of AC activation energies ($E_a$) obtained for the samples from the slope of $\sigma_{ac}$ versus $10^3/T$ at the frequency of 1MHz as illustrated in Fig. 6. The increase of applied field frequency enhances the electronic jumps between localized states, and consequently, the activation energy $E_a$decreases, which confirms the hopping conduction between the defect centers around Fermi level to be a dominant mechanism of conduction. This means that $\sigma_{ac}$at high frequencies is not thermally activated in a relatively wide range of temperatures. On the other hand, at lower frequencies and higher temperatures, the AC conductivity is temperature dependent, similar to that of DC conductivity. The activation energy is found to decrease while the conductivity increases with an increase in Cu content.

Since the conductivity is associated with an increase in the concentration of mobile electrons or polarons, indicating an increase in the concentration of $Cu^{2+}$ in the samples.

The frequency exponent (s) was obtained by the slope of the linear part of lnf versus $\sigma_{ac}$ plots for the present $Cu_{15}WO_3$ samples as shown in Fig.5e inset to Fig. 5d. The value of exponent (s) lies between 0 and 1, depending on temperature and materials. Thus, this independent of frequency and gives us information about the conduction mechanism for charge carriers in the materials. It was found to decrease from 0.817 to 0.145 with increasing temperature. This behaviour was associated with the correlated barrier hopping (CBH) model (Hutchins *et al.* 2007). In the CBH model, bipolaron has been proposed to interpret the frequency-dependent conductivity. This model does not explain the conductivity of samples at the high-temperature region, particularly in the low-frequency range. Therefore, CBH model can be used to describe temperature-dependent AC conductivity of the present samples at low-temperature region.
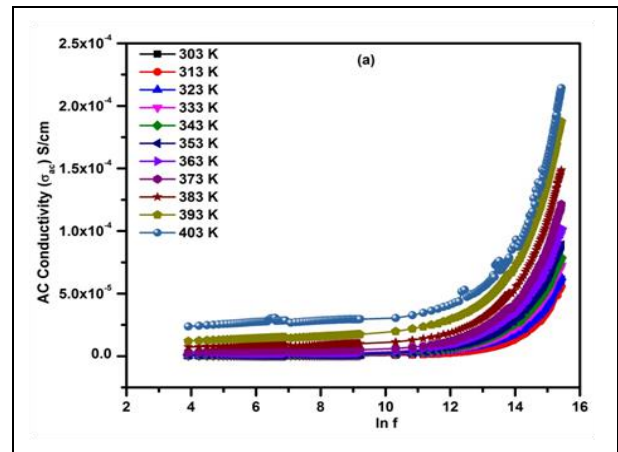


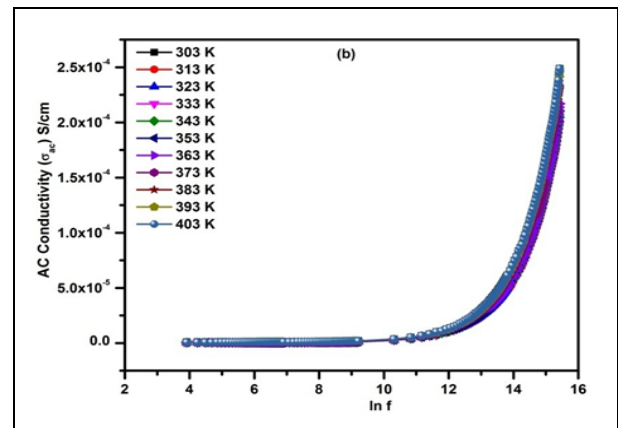**Fig. 5a: Frequency dependence of AC conductivity (σac) for WO₃**



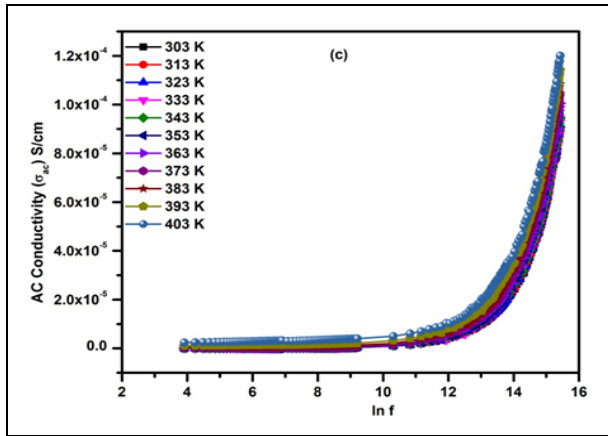**Fig. 5b: Frequency dependence of AC conductivity (σ ac) for 5 wt % Cu doped WO₃**

**Fig. 5c: Frequency dependence of AC conductivity (σ ac) for 10 wt % Cu doped WO₃**



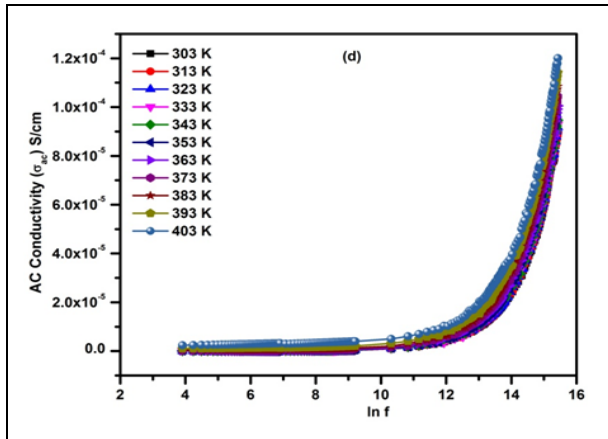**Fig. 5d: Frequency dependence of AC conductivity (σ ac) for 15 wt% Cu doped WO₃ at different temperature. Inset: Variation of frequency exponent (s) with a temperature of 15 wt% Cu doped WO₃**

### 3.3.3 Dielectric constant (ε') and dielectric loss (tan δ)

The dielectric constant (ε') of pure and doped WO₃ as a function of frequency in the range from 42Hz to 5MHz at various temperatures (303-403 K) is shown in Fig. 7. The value of the dielectric constant was found to increase with increasing temperature and at a higher temperature; it reaches maximum value, especially at lower frequencies for both the samples. Further, the higher dielectric constant value at lower frequencies, it decreases with increase in frequency and thereafter becomes constant at a very high frequency for all temperature. This type of behavior is in agreement with M–W (Maxwell–Wagner) model. In this model, a dielectric medium is composed of well-conducting grains, which are separated by poorly conducting and resistive grain boundaries. Therefore, an electric field is applied externally; the charge carriers can easily move within the grain and get accumulated at the grain boundaries as a result of large polarization and high dielectric constant produced in the sample (Wagner *et al.*

1913). The small conductivity at grain boundary contributes to the higher dielectric constant value at a low-frequency region. Additionally, the higher value of the dielectric constant can be explained on the basis of space charge/interfacial polarization, which occurs due to inhomogeneity of dielectric structure. In the present sample, the dopant Cu creates defects such as vacancies, porosities, the presence of oxygen etc. Meanwhile, Gupta *et al.* also found that the average grain size also played a crucial role in the dielectric constant (Gupta and Kumar, 2011). When average grain size decreases, the number of grain per unit volume increases. Hence, the number of electric dipoles per unit volume in the dielectric medium also increases, which increases the dielectric constant of the material. The smaller crystallite size of pure WO₃ has the maximum dielectric constant among doped samples. The dopant Cu is responsible for the dielectric constant value in the present samples. The dielectric constant decreases with the increase in frequency and then reach a constant value due to the fact that beyond a certain frequency of external field, the hopping between different metal ions ($W^{5+}$, $Cu^{2+}$) cannot follow the alternating field. The reduction of dielectric constant with frequency is natural because of the fact that any species contributing to polarizability is found to show lagging behind the alternating applied field at higher and higher (Reza Zamiri*et al.* 2014).
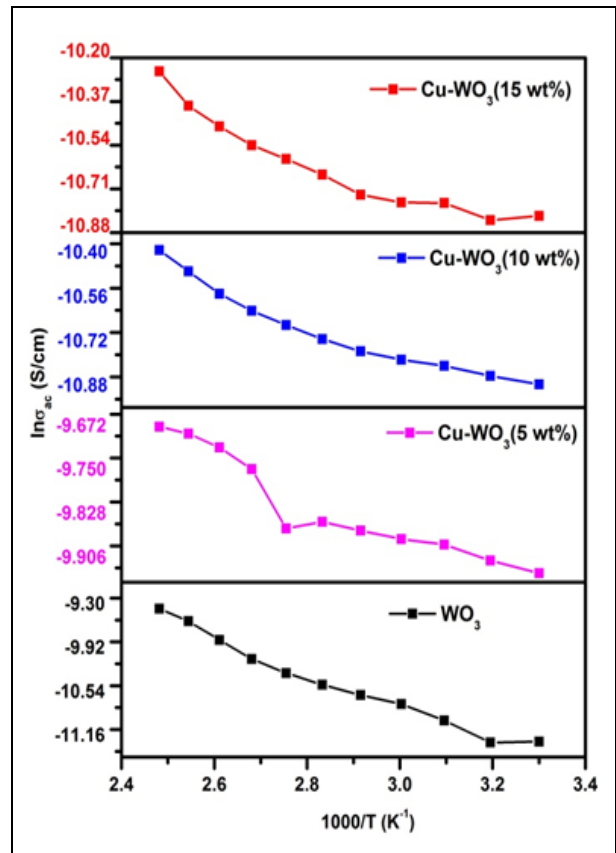


**Fig. 6: Arrhenius plot lnσ_ac versus $T^{1/3}$ for WO₃ and Cu doped WO₃**

### 3.3.3 Dielectric constant (ε') and dielectric loss (tan δ)

The dielectric constant (ε') of pure and doped $WO_3$ as a function of frequency in the range from 42Hz to 5MHz at various temperatures (303-403 K) is shown in Fig. 7. The value of the dielectric constant was found to increase with increasing temperature and at a higher temperature; it reaches the maximum value, especially at lower frequencies for both the samples. Further, the higher dielectric constant value at lower frequencies, it decreases with increase in frequency and thereafter becomes constant at a very high frequency for all temperature. This type of behaviour is in agreement with M–W (Maxwell–Wagner) model. In this model, a dielectric medium is composed of well-conducting grains, which are separated by poorly conducting and resistive grain boundaries. Therefore, an electric field is applied externally; the charge carriers can easily move within the grain and get accumulated at the grain boundaries as a result of large polarization and high dielectric constant produced in the sample (Wagner *et al.*1913). The small conductivity at grain boundary contributes to the higher dielectric constant value at a low-frequency region. Additionally, the higher value of the dielectric constant can be explained on the basis of space charge/interfacial polarization, which occurs due to the inhomogeneity of the dielectric structure. In the present sample, the dopant Cu creates defects such as vacancies, porosities, the presence of oxygen etc. Meanwhile, Gupta *et al.* also found that the average grain size also played a crucial role in the dielectric constant (Gupta and Kumar, 2011). When average grain size decreases, the number of grain per unit volume increases. Hence, the number of electric dipoles per unit volume in the dielectric medium also increases, which increases the dielectric constant of the material. The smaller crystallite size of pure $WO_3$ has the maximum dielectric constant among doped samples. The dopant Cu is responsible for the dielectric constant value in the present samples. The dielectric constant decreases with the increase in frequency and then reach a constant value due to the fact that beyond a certain frequency of external field, the hopping between different metal ions ($W^{5+}$, $Cu^{2+}$) cannot follow the alternating field. The reduction of dielectric constant with frequency is natural because of the fact that any species contributing to polarizability is found to show lagging behind the alternating applied field at higher and higher (Reza Zamiri*et al.* 2014).

Fig. 8 reveals that the value of dielectric loss (tan δ) is found to increase with the increase in temperature, especially at higher temperatures and at lower frequencies. The dielectric loss represents the dissipation of energy in the dielectric system. The tan δ values decrease with the increase of frequency and become almost frequency constant and independent at higher frequencies for all the samples, which may be due to space charge polarization. On the other hand, tan δ curves exhibit a peaking behavior for $WO_3$. The observed new

peaks at lower temperatures were observed and also noted that the height of the peak increases as the temperature increases. The observed peaks of tan δ versus frequency graphs can be explained according to the fact that a strong correlation between the conduction mechanism and the dielectric behavior exists in the sample.
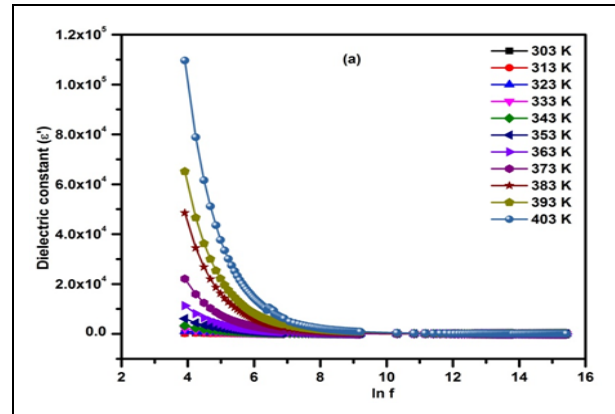


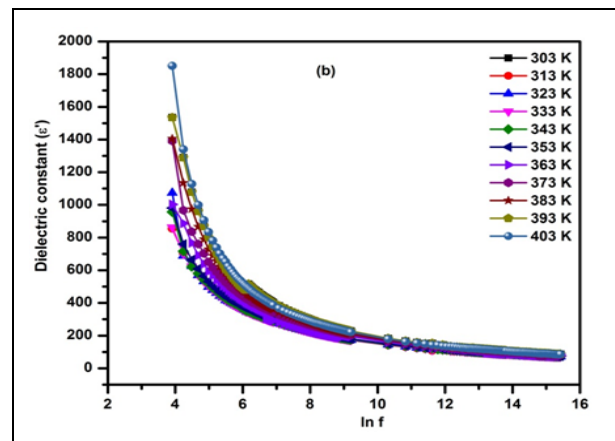**Fig. 7a: Frequency dependence of dielectric constant (ε') for $WO_3$**



**Fig. 7b: Frequency dependence of dielectric constant (ε') for 5 wt% Cu doped $WO_3$**
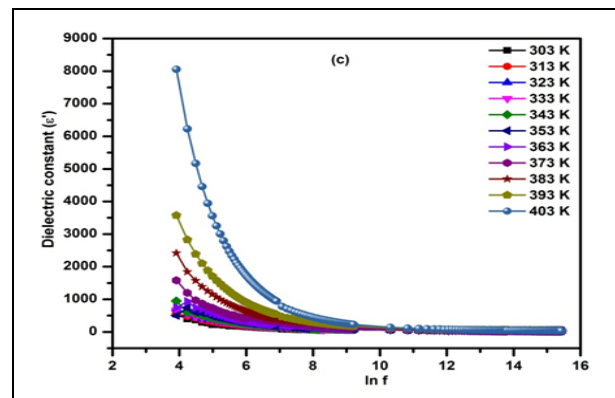


**Fig. 7c: Frequency dependence of dielectric constant (ε') for 10 wt% Cu doped $WO_3$**
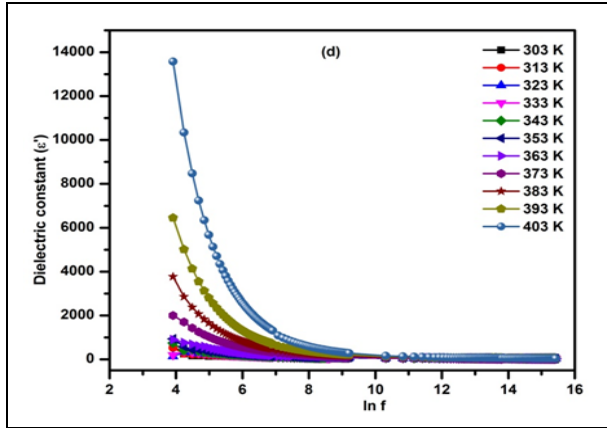
**Fig. 7d: Frequency dependence of dielectric constant (ε') for 15 wt% Cu doped WO₃ at different temperature.**

Therefore, a peak is expected when the hopping frequency of the electrons hopping between $W^{5+}$ and $W^{6+}$ ions is approximately equal to that of the externally applied field. Additionally, the observed peak of the pure $WO_3$ sample has been maximum exhibit loss which decreases after Cu doping and is gradual decreases in the higher frequency regime.
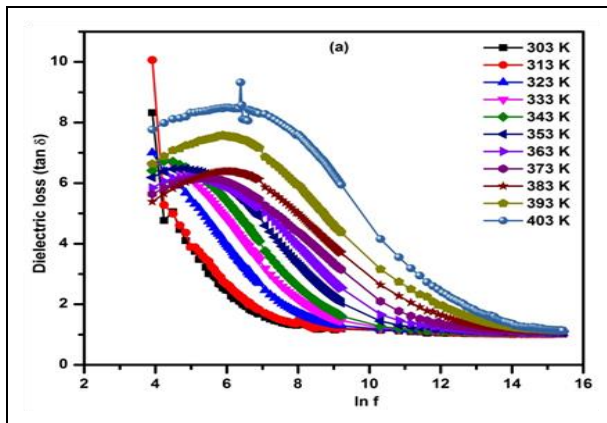


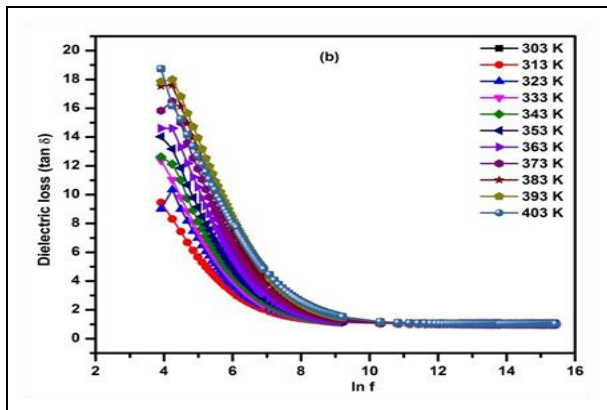**Fig. 8a: Frequency dependence of dielectric loss (tan δ) for WO₃**



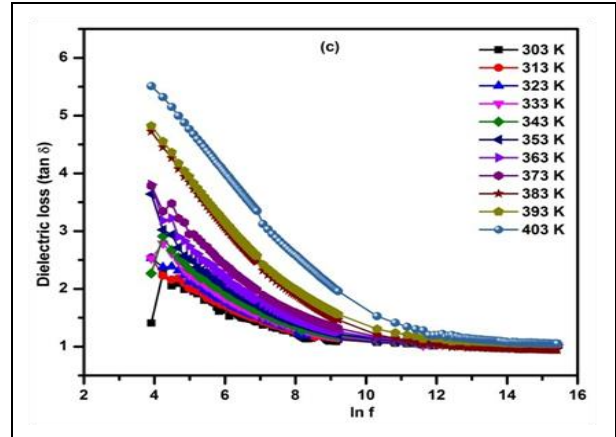**Fig. 8b: Frequency dependence of dielectric loss (tan δ) for 5 wt% Cu doped WO₃**



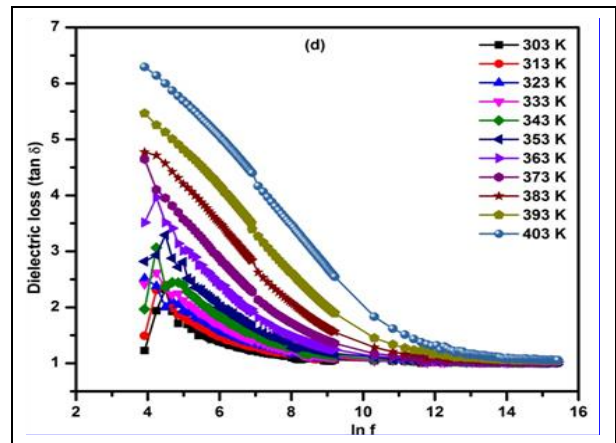**Fig. 8c: Frequency dependence of dielectric loss (tan δ) for 10 wt% Cu doped WO₃**



**Fig. 8d: Frequency dependence of dielectric loss (tan δ) for 15 wt% Cu doped WO3 at different temperature**

The measured $\sigma_{ac}$, ε' and tan δ increase as $Cu^{2+}$ ion substitution increases as a function of frequency at various temperature. The number of vacancies may be established at the tungsten site as Cu content increases. Such vacancies start on the thermal dissociation of oxygen, which in turn increases the number of electrons (Zaki, 2005). It will be helpful to increase the hopping process and can account for the increase in $\sigma_{ac}$, ε' and tan δ as Cu content increases. For that reason, it can be concluded that the Cu-doped $WO_3$ can be applied for high-frequency device applications.

## 4. CONCLUSION

In summary, Cu-doped $WO_3$ nanoparticles have been successfully synthesized by the wet chemical method. The structural and morphological studies revealed the presence of $Cu^{2+}$ had been completely incorporated in the $WO_3$. The small polaron hopping is observed in DC conductivity. The temperature of electrical conductivity was found to be thermally activated within 303-403 K. The electrical conductivity obeys Arrhenius behavior, and plot exposed activation

energies decreased with increasing wt% of Cu content indicates a thermally activated process. The calculated frequency exponent (s) is found to be less than one and decreased with the increase of temperature; consequently, the correlated barrier hopping (CBH) model is the most probable conduction mechanism for both the pure and Cu doped $WO_3$. AC conductivity of $WO_3$ nanoparticles is found to decreases with Cu doping. This reduction in conductivity could be due to the presence of tungsten interstitials and oxygen vacancies in $WO_3$ on Cu doping. Therefore, the incorporation of Cu ions in $WO_3$ lattice facilitates the formation of grain boundary defect leading to the blockage of the flow of charge carriers. This, in turn, decreases the conductivity of the system on doping. The frequency dependence of the dielectric study of the prepared samples showed the dielectric constant and dielectric loss at different temperature due to wt% of Cu-dopant. From the observation, the simple and low-cost fabrication of Cu-doped $WO_3$ nanoparticles and its interesting electrical and dielectric properties of the material used to make nanoelectronic devices such as a capacitor, gas sensing, humidity sensing, absorption, etc.

## FUNDING

## CONFLICTS OF INTEREST

The authors declare that there is no conflict of interest.

## COPYRIGHT

## REFERENCES

Ahsan, M.,Tesfamichael, T.,Ionescu, M., Bell, J. andMotta, N., Low temperature CO sensitive nanostructured $WO_3$ thin films doped with Fe, *Sensor. Actuator. B.,* 162(1), 14– 21(2012).
https://doi.org/10.1016/j.snb.2011.11.038

Changhua Wang, XintongZhang , Bo Yuan, Yuxi Wang, Panpan Sun , Dan Wang, Yongan Wei, Yichun Liu: Multi-heterojunction photocatalysts based on $WO_3$nanorods: Structural, design and optimization for enhanced photocatalytic activity under visible light, *Chem. Eng. J.*, 237, 29-37(2014).
https://doi.org/10.1016/j.cej.2013.10.003

Cholsong Pang, Ji Luo, ZhimengGuo, Min Guo, Ting Hou, Inhibition of tungsten particle growth during reduction of V-doped $WO_3$ nanoparticles prepared by co-precipitation method, *Int. J. Refract. Met. H.,* 28, 343–348(2010).

Danine, A., Cojocaru, L., Faure, C., Olivier, C., Toupance, T., Campet, G. and Rougier, A., Room Temperature UV treated $WO_3$ thin films for electrochromic devices on paper substrate, *Electrochim. Acta.*, 129, 113-119(2014).
https://doi.org/10.1016/j.electacta.2014.02.028

El-Nahass, M. M., Ali, H. A. M.,Saadeldin, M. and Zaghllol, M., AC conductivity and dielectric properties of bulk tungsten trioxide ($WO_3$), *Physica. B.*, 407(22), 4453-4457(2012).
https://doi.org/10.1016/j.physb.2012.07.043

Gartstein, Y. N. and Conwell, E. M., High-field hopping mobility in molecular systems with spatially correlated energetic disorder,*Chem. Phys. Lett.*, 245(4-5), 351-358(1995).
https://doi.org/10.1016/0009-2614(95)01031-4

Gaury,J., Kelder, E. M., Bychkov, E. andBiskos, G., Characterization of Nb-doped $WO_3$ thin films produced by Electrostatic Spray Deposition, *Thin Solid Films*, 534, 32–39(2013).
https://doi.org/10.1016/j.tsf.2013.01.080

Georg, A., Georg, A., Graf, W. and Wittwer, V., Switchable windows with tungsten oxide, *Vacuum*, 82(7), 730–735(2008).
https://doi.org/10.1016/j.vacuum.2007.10.020

Gupta, M. K. and Kumar, B.,Enhanced ferroelectric, dielectric and optical behavior in Li-doped ZnOnanorods, *J. Alloy. Compd.,* 509(23), L208-L212(2011).
https://doi.org/10.1016/j.jallcom.2011.03.119

Hao Zhou, Dong-Yao Xu, Hai-Qing Zuo,Wei Liu, Shuang Lin, Preparation of Flower-Like Cu-$WO_3$ Nanostructures and Their Acetone Gas Sensing Performance, *J. Chem.*, 2015, 382087(2015).
https://doi.org/10.1155/2015/382087

Hubalek, J.,Malysz, K., Prasek,J., Vilanova, X., Ivanov, P.,Llobet, E.,Brezmes, J., Correig, X. andSverák, Z., Pt-loaded $Al_2O_3$ catalytic filters for screen-printed $WO_3$ sensors highly selective to benzene, *Sensor. Actuator. B.*, 101(3), 277–283(2004).
https://doi.org/10.1016/j.snb.2004.01.015

Hui Song, Yaguang Li, Zirui Lou, Mu Xiao, Liang Hu, Zhizhen Ye, Liping Zhu, Synthesis of Fe-doped $WO_3$ nanostructures with high visible-light-driven photocatalytic activities, *Appl.Catal. B: Environ.*, 166–167, 112–120(2015).
https://doi.org/10.1016/j.apcatb.2014.11.020

Huijuan Xia, Yan Wang, Fanhong Kong, Shurong Wang, Baolin Zhu, XianzhiGuo, Jun Zhang, Yanmei Wang, Shihua Wu, Au-doped $WO_3$-based sensor for $NO_2$ detection at low operating temperature, *Sensor. Actuator. B.*, 134, 133–139(2008).
https://doi.org/10.1016/j.snb.2008.04.018

Huijuan Xia, Yan Wang, Fanhong Kong, Shurong Wang, Baolin Zhu, XianzhiGuo, Jun Zhang, Yanmei Wang, Shihua Wu, Au-doped WO₃-based sensor for NO₂ detection at low operating temperature, *Sensor. Actuator. B.*, 134(1), 133–139(2008).
https://doi.org/10.1016/j.snb.2008.04.018

Hutchins, M. G., Abu-Alkhair, O., El-Nahass, M. M. and Abdel-Hady, K.,Electrical conductivity and dielectric relaxation in non-crystalline films of tungsten trioxide, *J. Non-Cryst.Solids.*, 353(44-46), 4137–4142(2007).
https://doi.org/10.1016/j.jnoncrysol.2007.06.042

Jonscher, K., Dielectric Relaxation in Solids, Chelsea Dielectric Press, London, 1983.

Kuzmin, A.,Anspoks, A.,Kalinko, A.,Kalinko, A. and Kalendarev, R., X-ray absorption spectroscopy of Cu-doped WO₃ films for use in electrochemical metallization cell memory, *J. Non-Cryst. Solids.*, 401, 87-91(2014).
https://doi.org/10.1016/j.jnoncrysol.2014.01.022

Mingshui Yao, Qiaohong Li, GuolinHou, Chen Lu, Benli Cheng, KechenWu,Gang Xu, FangliYnan, Fei Ding, Yunfa Chen,Dopant-Controlled Morphology Evolution of WO₃Polyhedra Synthesized by RF Thermal Plasma and Their Sensing Properties, *ACS Appl. Mater. Interfaces.*, 7(4), 2856–2866(2015).
https://doi.org/10.1021/am5081277

Mott, N. F. and Davis, E. A., Electronic Process in Non-Crystalline Materials, Clarendon Press, Oxford, 1972.
https://doi.org/10.1002/crat.19720070420

Reza Zamiri, Ajay Kaushal, AvitoRebelo J.M. F. Ferreira, Er doped ZnOnanoplates: Synthesis, optical and dielectric Properties, *Ceram. Int.,* 40(1), 1635-1639(2014).
https://doi.org/10.1016/j.ceramint.2013.07.054

Shenmin Zhu, Xinye Liu, Zhixin Chen, ChunjiaoLiu,ChuanliangFeng,JiajunGu,Qinglei Liu, Di Zhang, Synthesis of Cu-doped WO₃ materials with photonic structures for high performance sensors for high performance sensors, *J. Mater. Chem.*, 20, 9126–9132 (2010).
https://doi.org/10.1039/C0JM02113J

Shumaila, G. B.,Lakshmi, V. S., Masood Alam, Azher M. Siddiqui, Zulfequar, M. and Husain, M., Synthesis and characterization of Se doped polyaniline, *Curr.Appl.Phys.*, 11(2), 217-222(2011).
https://doi.org/10.1016/j.cap.2010.07.010

Simpson, C. andCordaro, J. F., Characterization of deep levels in zinc oxide,*J. Appl. Phys.*, 63(5), 1781-1783(1988).
https://doi.org/10.1063/1.339919

SomayehFardindoost, AzamIrajizad, FereshtehRahimi, RoghayehGhasempour, Pd doped WO₃ films prepared by sol-gel process for hydrogen sensing, *Int. J. Hydrogen Energy*, 35(2), 854– 860(2010).
https://doi.org/10.1016/j.ijhydene.2009.11.033

Upadhyay, B., Mishra, R. K. and Sahay, P. P.,Structural and alcohol response characteristics of Sn-doped WO3 nanosheets,*Sensor. Actuator. B.,* 193, 19–27(2014).
https://doi.org/10.1016/j.snb.2013.11.049

Wagner, K. W.,Zurtheorie der unvollkommenendielektrika, *Annalen der Physik* 345(5), 817-855(1913).
https://doi.org/10.1002/andp.19133450502

Wang X,, Song C, Geng K, Zeng F, Pan F: Photoluminescence and Raman scattering of Cu-doped ZnO films prepared by magnetron sputtering,*Appl. Surf. Sci.*, 253, 6905–6909(2007).
https://doi.org/10.1016/j.apsusc.2007.02.013

Wang, W., Research on Surface Doped Tungsten Oxide Gas- Sensing Mechanism, Tianjin University, TanJin, China, 2011.

Wen Zeng, Chining Dong, Bin Miao, He Zhang, Sibo Xu, Xuezheng Ding and Shahid Hussain, Preparation, characterization and gas sensing properties of sub-micron porous WO₃ spheres, *Mater. Lett.*, 117, 41–44(2014).
https://doi.org/10.1016/j.matlet.2013.11.080

Zaki, H. M., AC conductivity and frequency dependence of the dielectric properties for copper doped magnetite, *Physica B*, 363(1-4), 232–244(2005).
https://doi.org/10.1016/j.physb.2005.03.026

Zhiyang He, Qiao Liu, HuilinHou, Fengmei Gao, Bin Tang, Weiyou Yang, Tailored Electrospinning of WO₃Nanobelts as Efficient Ultraviolet Photodetectors with Photo-Dark Current Ratios up to 1000, *ACS Appl. Mater. Interfaces.*, 7(20), 10878–10885(2015).
https://doi.org/10.1021/acsami.5b02020